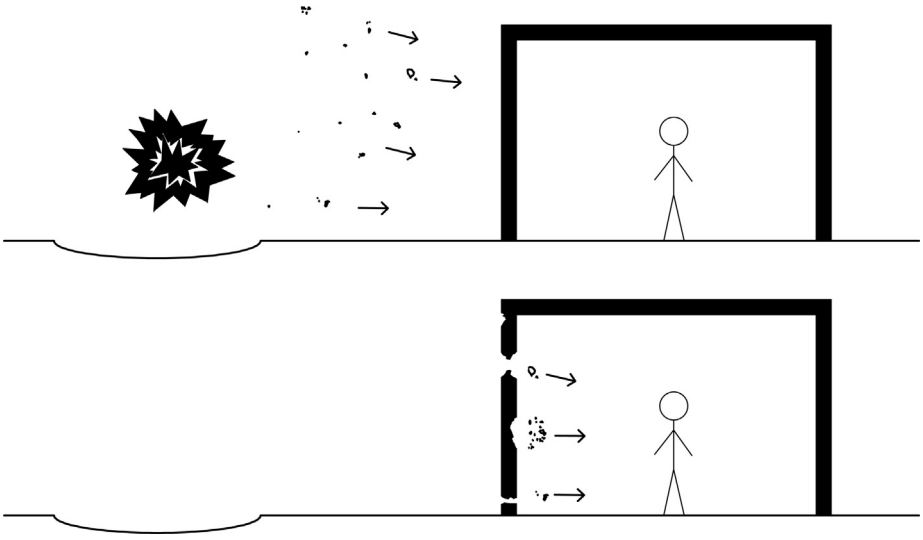

Fig. 1. Explosion-generated projectiles.

2. Mixture optimization

2.1. Mix design and sample preparation

During the mixing of UHPC, it is very important to achieve good workability, particle distribution and packing density. In comparison to normal strength concrete, UHPC contains more constituents and finer particles. Several researchers recommend [6,13,14] to mix all fine dry particles first before adding water and high-range water reducer (HRWR). It is because small particles tend to agglomerate and it is easier to break these chunks when the particles are dry. The specific mixing procedure was as follows: In the first step both types of aggregate (A) and silica fume (SF) were mixed for 5 min. In the second step cement (C) and glass powder (GP) were mixed for another 5 min. At the end of the procedure water and HRWR were added. The addition of HRWR was gradual. The mixture became fully workable after another 5 min.

In case of UHPFRC fibers were added gradually into the flowable mixture to avoid chunks formation during additional 5 min of mixing. The shear action of fibers helped to destroy any remaining agglomerates in the mixture, thus improving workability. The total mixing time was 15 min for UHPC mixtures and 20 min for UHPFRC. A horizontal, low rotation speed mixer with a capacity of 50 l was used to prepare the samples.

2.2. Cementitious matrix design and optimization

In the first phase of the research, several concrete mixtures without fibers were produced to find the best combination of constituents with respect to maximal compressive strength and workability. High particle packing density is a key property of ultra-high compressive strength of concrete. Therefore the mixture design was based on optimizing the particle packing density of S, SF, GP and C as well as alternating various sand fractions. In total 24 mixture designs were tested. Flexural strength was evaluated on 40 × 40 × 160 mm prisms and compressive strength was determined on the halves of these prisms following CSN EN 1015-11. Workability was tested according to CSN EN 1015-3 using standard flow-table test.

The first mixture was designed following the proportions of C:SF:GP recommended by Wille et al. [2] as 1:0.25:0.25 with a water-binder (w/b) ratio of 0.2. Subsequent changes in the most important parameters such as HRWR, water, amount of A, SF, and GP led to an optimized cementitious matrix in terms of compressive strength and workability. From the 24 tested mixtures, two best performing cementitious matrix compositions denoted as UHPC2 and UHPC3 are shown in Table 1 along with the first starting mixture (UHPC1). Table 1 also shows basic material properties of the selected mixtures. In the average spread row a diameter of paste spread measured after filling and removing the standard cone and impacting the table 15 times is compared.

2.3. Fiber addition

In the second step of the optimization process straight steel fibers were added up to 3% of volume in replacement of the equivalent volume of coarser sand to the best performing mixture i.e. UHPC3 and forming UHPFRC 3 mixtures. Straight fibers were used because it is known that they provide a good trade-off between tensile properties and workability of the composite [13]. The fibers were 13 mm long with a diameter of 0.15 mm and tensile strength of 2800 MPa. Mixture proportions can be found in Table 2. The second number after the type of matrix denotes the fiber content by volume. For instance UHPFRC 3-2 means mixture containing 2% of fibers which is based on the UHPC 3 matrix design. The mixing procedure was the same as for previous samples. For each mixture (UHPC 3, UHPFRC 3-1, UHPFRC 3-2, UHPFRC 3-3) three cylinders with a diameter of 100 mm and height of 200 mm, three dog-bone

Table 1
Design of mixtures without fibers.

Type of component	UHPC1	UHPC2	UHPC3
	Proportions by weight		
(C) Cement CEM I 52,5R	1	1	1
(SF) Silica fume	0.25	0.25	0.25
(GP) Glass powder	0.25	0.25	0.25
(W) Water	0.25	0.22	0.22
(HRWR): Sika SVC 20 Gold	0.050	–	0.031
(HRWR): Sika ViscoCrete 20He	–	–	0.019
(HRWR): Sika ViscoCrete 30He	–	0.025	–
(HRWR): Sika ViscoCrete 1035	–	0.025	–
(A) Fine sand 0.1/0.6 mm	0.42	0.42	0.42
(A) Fine sand 0.3/0.8 mm	1	1	1
(w/b) Water/binder ratio	0.2	0.176	0.176
Average spread (workability) [mm]	140	150	150
Avg. compr. strength [MPa]	110.0	132.2	141.9
Avg. flexural. strength [MPa]	17.6	20.8	22.1

Table 2
Final mixture design including fibers.

Type of component	UHPFRC 3-1	UHPFRC 3-2	UHPFRC 3-3
	Proportions by weight		
(C) Cement CEM I 52,5R	1	1	1
(SF) Silica fume	0.25	0.25	0.25
(GP) Glass powder	0.25	0.25	0.25
(W) Water	0.22	0.22	0.22
(HRWR): Sika SVC 20 Gold	0.031	0.031	0.031
(HRWR): Sika ViscoCrete 20He	0.019	0.019	0.019
(A) Fine sand 0.1/0.6 mm	0.42	0.42	0.42
(A) Fine sand 0.3/0.8 mm	0.9	0.8	0.7
(w/b) Water/binder ratio	0.176	0.176	0.176
(F) Fibers	0.1	0.2	0.3

specimens, three 40 × 40 × 160 mm prisms and two 300 × 400 × 50 mm slabs were casted.

3. Mechanical properties

3.1. Compressive strength and modulus of elasticity

Compressive strength and secant modulus of elasticity were measured on cylinders with 100 mm diameter and height of 200 mm. Because the strength of the best available capping material (100 MPa) was significantly lower than the expected measured strengths, tops of the cylinders were cut off and grinded. Compressive strength was measured on cylinders by monotonic increments of load with average speed of 36 MPa/min up to the level of 70% of the expected compressive strength. At this point loading was switched to deformation control with a speed of 0.48 mm/min for about 2 min in order to measure peak and post peak behaviour. In the softening branch speed was increased to 1.2 mm/min.

Modulus of elasticity was measured using two extensometers with a 100 mm base, attached to the sides of the cylinder specimen. A hydraulic loading machine DSM2500-100 was used and the loading procedure was stress controlled. In the first step the specimens were loaded to 1/3 of expected maximal compressive strength – in this case 50 MPa – for 60 s. Afterwards the specimens were unloaded to 5 MPa. This procedure was repeated three times. The secant modulus of elasticity was calculated from the third unloading cycle. In the second step, the specimens were loaded until failure and compressive strength was determined.

3.2. Tensile strength

Direct tensile tests were carried out on dog-bone shaped specimens without a notch. The length of the specimens was 330 mm and the cross-section of the narrowed part was 30 × 30 mm. The specimens were categorized with respect to volumetric content of steel fibers as outlined in Table 2. Three specimens from each category were tested. All specimens were cast in layers which led to alignment of fibers in the direction of the applied load.

The direct tensile tests were performed on MTS loading machine. The specimens were mounted into specially developed grips. The extension in the elastic region was measured with two strain gauges glued on both narrow sides. After the localization of a crack the extension was measured with two LVDTs mounted with a special frame on the dog-bone specimen. The loading speed was 0.1 mm/min for specimens without fibers. In case of specimens containing fibers the loading was performed in two steps. The loading speed in the first step was 0.3 mm/min until the load decreased to approximately 70% of the maximal load. In the second step the loading speed was increased to 0.5 mm/min. This loading procedure was chosen in order to speed up the test as deformation after the crack opening was in order of magnitude larger than deformation measured until peak load.

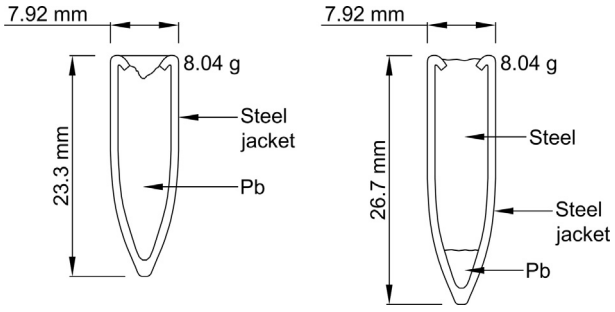

Fig. 2. Deformable and non-deformable steel-jacketed projectile.

3.3. Projectile impact

Resistance to impact loading was performed on rectangular slabs with dimensions 300 × 400 mm and thickness of 50 mm. As the presence of reinforcing bars has negligible effect on the perforation resistance of the slabs as described by Hanchak et al. [15], no reinforcing bars were utilized to construct the specimens. Impact was simulated as a hit of deformable or non-deformable give nose projectile (Fig. 2). Distance to the slab was 20 m and muzzle velocity was measured with a shooting chronograph located approximately 2 m from the gun muzzle. The weight of the projectile was 124 grains (8.04 g) and the average muzzle velocity was 710 m/s. In total 18 slabs were tested for impact loading. Extent of damage caused by the impact was defined by the penetration depth and crater diameter. Slabs made of UHPC 3, UHPFRC 3-1, 3-2, 3-3 were tested. In order to compare UHPC and UHPFRC with commonly used mixtures another two concretes were examined – normal strength concrete (NSC) and conventional fiber reinforced concrete (FRC).

FRC slabs were constructed using maximal aggregate size of 8 mm and hooked steel fibers with aspect (length-to-diameter) ratio of 85 and a length of 30 mm. The fibers had a nominal tensile strength of 2300 MPa. The hooked ends are generally considered as best form of anchorage. Average compressive strengths of FRC and NSC were determined to be 57 MPa and 48 MPa, respectively.

Each test specimen was placed in a special mount developed for the purpose of this study in order to prevent movement of the specimen during the impact. The mount was provided with four screws located in the corner of the specimen approximately 50 mm from both edges in order to simulate point supports. Each specimen was placed in the mount and the projectile hit the center of the specimen under the right angle with small deviation around 3° which was considered as negligible.

4. Results and discussion

4.1. Mechanical properties

Table 3 shows workability, compressive strength, flexural strength, direct tensile strength and secant modulus of elasticity of the developed UHPFRC mixtures with respect to fiber content. It can be seen that the average highest compressive strength of 151.7 MPa was achieved for 2% of fiber volumetric content. In correspondence with that the highest average secant modulus of elasticity of 56.9 GPa was measured for 2% fiber volume. The

Table 3
Average mechanical properties of the UHPFRC mixtures.

	UHPC 3	UHPFRC 3-1	UHPFRC 3-2	UHPFRC 3-3
Workability – spread [mm]	200	220	225	190
Compressive strength [MPa]	132.4	148.5	151.7	148.1
Flexural strength [MPa]	9.9	27.0	40.1	47.5
Direct tensile strength [MPa]	6.6	7.1	10.4	11.7
Modulus of elasticity [GPa]	41.1	45.1	56.3	51.5

highest flexural and direct tensile strength were achieved for samples containing 3% of fibers by volume (Fig. 2).

Direct tensile strength measurement results are presented in Fig. 3. The results of the uniaxial tensile tests of specimens containing 0% and 1% of fibers are presented in the top section of Fig. 3. Results for specimens containing 2% and 3% of fibers are shown in the bottom section of Fig. 3. Horizontally is Fig. 3 divided into two parts that are typical for UHPFRC behaviour: a) linear-elastic and strain hardening part, which includes the linear-elastic stress rise and the strain hardening part of stress–strain diagram. It is possible to say, that the energy dissipation is volumetric in this part; b) the softening part in which the energy is dissipated in a localized crack at the crack surface.

Fig. 3a shows the stress–strain relationship in the strain hardening part of the curve. The stress is calculated by dividing the measured force by the reduced cross-section of the dog-bone specimen (30 × 30 mm). Strain values were determined from the average strain measured by two strain gauges, which were glued on the side of the specimen. Fig. 3b provides the relation between stress and total crack width during softening. The total crack width was determined as an average from two LVDTs which spanned over the entire reduced cross-section of the specimen. The average apparent strain at the end of strain hardening region was 140 μm/m for samples with 1% of fibers, 1478 μm/m for samples with 2% of fibers and 1885 μm/m for samples containing 3% of fibers. Wuest et al. [16] used similar types of fibers (2.5% vol.) and measured 2400 μm/m at the end of strain hardening region at a tensile strength of 14.2 MPa which is more than observed in this study where the average direct tensile strength was 7.1 MPa, 10.4 MPa and 11.7 MPa for UHPFRC 3-1, 3-2 and 3-3 respectively.

4.2. Response to projectile impact

The results of the impact tests including response type, muzzle velocities, average crater diameter, penetration depth, spalling and scabbing are presented in Tables 4–6. Response type was classified in accordance with the convention used in Vossoughi et al. [17] as perforated – P (the projectile passed through the specimen entirely), perforation limit – PL (projectile was stuck), perforated and then bounced – PB (the projectile went through the slab and then bounced back) and unperforated – UP (panel was punched but the projectile bounced back).

It was verified that increase of the fiber content has no significant effect on the penetration depth in case of the deformable projectile impact. Perforation through the slab occurred only in the case of UHPC specimen. In case of UHPFRC slabs were not perforated and the projectile bounced back. The average penetration depth was reduced from 20.5 mm to 20.0 mm and 19.0 mm for

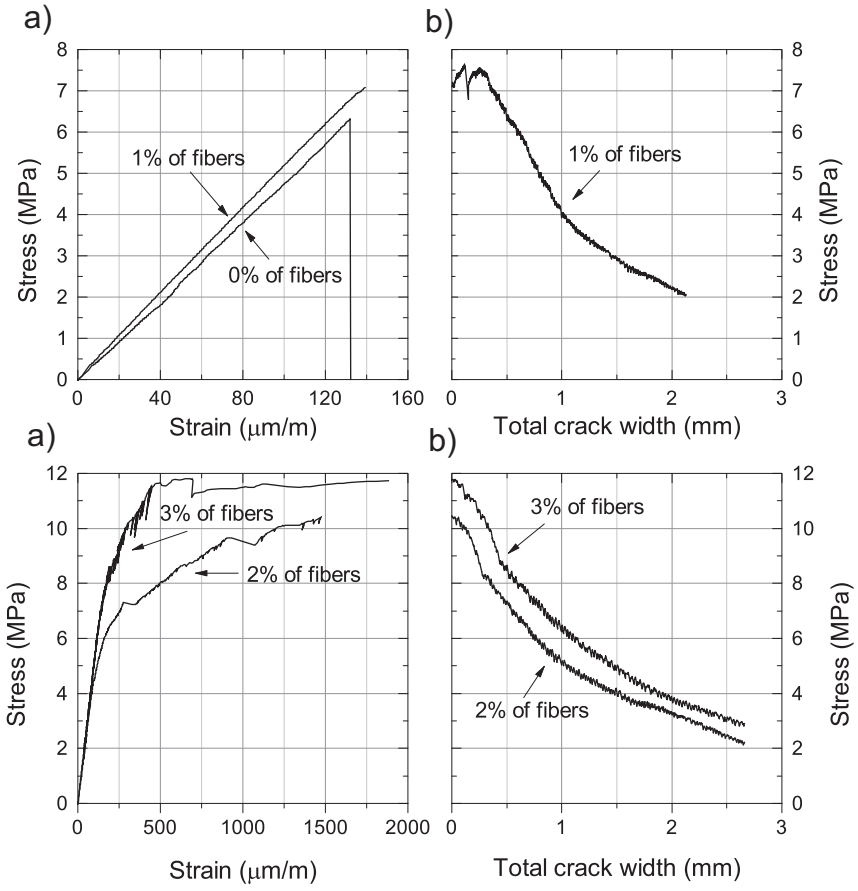

Fig. 3. Tensile behaviour of UHPC and UHPFRC.

Table 4
Response and damage assessment for the UHPC and UHPFRC mixtures subjected to deformable projectile impact.

Type of concrete	UHPC 3		UHPFRC 3-1		UHPFRC 3-2		UHPFRC 3-3	
Type of projectile	D							
Fiber content [%]	0	0	1	1	2	2	3	3
Specimen number	1	2	1	2	1	2	1	2
Muzzle velocity [m/s]	710	714	715	728	692	706	716	718
Response type	P	P	UP	UP	UP	UP	UP	UP
Crater – front side [mm]	–	148	68	101	80	68	83	63
Penetration depth [mm]	50	50	20	21	19	21	19	19
Mass loss [g]	–	–	53	122	63	44	50	170
Spalling [g]	–	–	53	108	63	44	50	85
Scabbing [g]	–	–	0	14	0	0	0	85

Table 5
Response and damage assessment for UHPFRC mixtures containing 2% of fibers subjected to both deformable and non-deformable projectile impact.

Type of concrete	UHPFRC 3-2							
Type of projectile	N-D				D			
Specimen number	1	2	3	4	5	6	1	2
Muzzle velocity [m/s]	712	706	706	718	721	718	683	709
Response type	PL	P	P	PL	P	PL	UP	UP
Crater – front side [mm]	77	63	68	80	81	94	62	81
Crater – rear side [mm]	65	100[a]	87	108[a]	74	90[a]	118[a]	126[a]
Mass loss [g]	46	35	129	32	90	32	41	63

[a] Fragment was still attached to the slab.

UHPFRC slabs as the content of fibers increased from 1% to 2% and 3%, respectively (Table 4). Therefore, it is evident that increasing the fiber content beyond 1% has only minor effect on penetration depth.

The crater diameters in UHPFRC mixtures were 42–50% smaller than those in UHPC mixtures (i.e. 0% of fibers). The results showed, that the implementation of fibers reduced the crater diameter significantly, however increase of fiber content beyond 2% has no further effect on crater diameter (Table 4).

Difference between the UHPFRC 3-2 and UHPFRC 3-3 in terms of response to deformable projectile impact was insignificant. Hence 2% fiber content by volume was found to be optimal. Further on, slabs with 2% of fiber content (UHPFRC 3-2) were subjected to non-deformable projectile impact. In case of specimen number 2, 3 and 5 (Table 5) the projectile passed through the slab entirely. In case of specimen number 1, 4 and 6 (Table 5) the projectile got stuck in the slab (Fig. 4).

Perforation occurred in every case of NSC as well as traditional FRC during both deformable and non-deformable projectile impact.

Table 6
Response and damage assessment for NSC and FRC mixtures subjected to both deformable and non-deformable projectile impact.

Type of concrete	NSC		FRC							
Type of projectile	D	N-D	D				N-D			
Specimen number	1	1	1	2	3	4	1	2	3	4
Muzzle velocity [m/s]	704	719	704	705	700	719	706	708	710	715
Response type	P	P	P	P	P	P	P	P	P	P
Crater – front side [mm]	88	74	75	74	78	61	61	66	53	81
Crater – rear side [mm]	141	119	98	97	71	94	91	91	79	85
Mass loss [g]	569	283	209	222	201	175	134	129	126	130

Fig. 4. Perforation limit: tip of the non-deformable projectile protrudes from the back side of the 50 mm thin UHPFRC 3-2 slab.

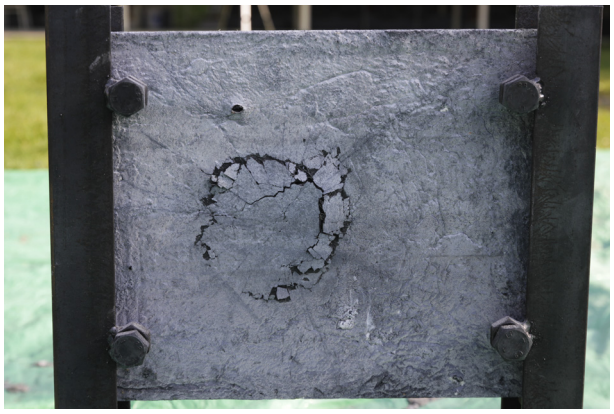

Fig. 5. Borders of the crater on the back side of the 50 mm thin UHPFRC 3-2 slab after deformable projectile impact (fragment is still attached to the slab).

Average mass loss in case of FRC was determined to be 202 g and 130 g for deformable and non-deformable projectile impact, respectively (Table 6). In case of UHPFRC 3-2 the average mass loss was determined to be 52 g and 61 g for deformable and non-deformable projectile impact, respectively (Table 5). Thus, implementation of UHPFRC can decrease flying debris down to 25% in comparison with conventional FRC.

In a few cases of UHPFRC 3-2 slabs the back side fragment was still attached to the slab after the projectile impact (Fig. 5) which decreased the average value of mass loss significantly. It was verified experimentally that UHPFRC has much better resistance to projectile impact in terms of both response type and mass loss. Some non-deformable projectiles were intercepted even by the 50 mm thin UHPFRC 3-2 slab and, in addition, in a few cases back side fragment was still attached to the slab. Hence, using UHPFRC may result in higher safety and security of civil infrastructure.

5. Conclusions and further outlook

The research described herein has shown that it is possible and relatively simple to develop a UHPFRC without the need for special curing such as heat or pressure. It was also shown that it is possible to use standard laboratory equipment such as a horizontal-pan mixer for preparing high performance cementitious composites. However, the strict control of the mixing procedure is essential and especially mixing times must be strictly adhered to. The initial strategy was to increase workability by optimizing the packing density of the mixture and using different types of HRWR. A spread

of the paste measured during the simple flow-table test was found to provide good indication of workability. In addition, results from three-point bending and compressive strength tests were utilized during the optimization process. All materials used in this research were commercially available in the Czech Republic.

The main findings of our research are as follows:

- An optimization of ultra-high performance cementitious composite was undertaken comprising laboratory tests on 24 mixtures with respect to its compressive strength, flexural strength and workability.
- Addition of fibers to the mixture increased the mechanical properties of the UHPFRC. However, more than 2% of fiber volumetric content decreased the compressive strength and modulus of elasticity.
- Direct tensile strength of the UHPFRC seemed to increase gradually with increasing content of fibers up to the 3%.
- With an increase in target mechanical parameters, UHPC and UHPFRC became much more sensitive to quality of the components, the dispersion of the particles, the mixing procedure, the specimen preparation and the curing.
- Addition of high strength fibers to the mixture enhanced the impact behaviour in terms of the penetration depth compared to their plain concrete counterparts. However, any further increase of the fiber content beyond 1% had no significant effect on the penetration depth of the projectile.
- In case of UHPFRC slabs the crater diameter decreased by 42%–50% compared to plain UHPC specimens. Further increase of fiber content beyond 2% had no effect on reducing the crater diameter, as diameter of the crater had a tendency to remain constant within 2% and 3% of fiber content.
- Based on the results presented herein, it can be concluded that the addition of high strength fibers enhanced the resistance to impact loading. It was found that the optimal amount of fiber content with respect to the mechanical properties, workability and resistance to projectile impact lies around 2% by volume.
- It was verified that UHPFRC has much greater resistance to impact loading compared to traditional FRC. Thus, implementation of UHPFRC may result in highly resistant concrete elements such as cladding panels and walls in modern protective structures while maintaining its standard thicknesses and appearance.
- The future research will focus on the measurement of fracture energy of UHPFRC under different strain rates and on further optimization of the matrix composition.

Acknowledgements

The authors gratefully acknowledge the support provided by the Czech Science Foundation under the project No. P104/12/0791: Fiber Reinforced Cement Composites for High Temperature Applications. The authors would like to acknowledge the assistance of the technical staff of the Experimental Centre, CTU in Prague and students who participated on the project. Namely Jan Zatloukal, Tomáš Vavřiník, Marek Piškytl and Jaroslav Pokorný.

References

[1] Cauberg N, Piérard J, Remy O. Ultra high performance concrete: mix design and practical applications; 2008.
[2] Wille K, Naaman AE, Parra-Montesinos GJ. Ultra-high performance concrete with compressive strength exceeding 150 MPa (22 ksi): a simpler way. ACI Mater J 2011;108:46–54.
[3] Graybeal BA. Compressive behavior of ultra-high-performance fiber-reinforced concrete. ACI Mater J 2007;104:146–52.
[4] Habel K, Charron J, Braike S, Hooton RD, Gauvreau P, Massicotte B. Ultra-high performance fibre reinforced concrete mix design in central Canada. Can J Civil Eng 2008;35:217–24.
[5] Rossi P, Arca A, Parant E, Fakhri P. Bending and compressive behaviours of a new cement composite. Cem Concr Res 2005;35:27–33.
[6] Habel K, Gauvreau P. Response of ultra-high performance fiber reinforced concrete (UHPFRC) to impact and static loading. Cem Concr Compos 2008;30:938–46.
[7] Bindiganavile V, Banthia N, Aarup B. Impact response of ultra-high-strength fiber-reinforced cement composite. ACI Mater J 2002;99:543–8.
[8] Zhang M, Shim V, Lu G, Chew C. Resistance of high-strength concrete to projectile impact. Int J Impact Eng 2005;31:825–41.
[9] Wang N, Mindess S, Ko K. Fibre reinforced concrete beams under impact loading. Cem Concr Res 1996;26:363–76.
[10] Farnam Y, Mohammadi S, Shekarchi M. Experimental and numerical investigations of low velocity impact behavior of high-performance fiber-reinforced cement based composite. Int J Impact Eng 2010;37:220–9.
[11] Maalej M, Quek ST, Zhang J. Behavior of hybrid-fiber engineered cementitious composites subjected to dynamic tensile loading and projectile impact. J Mat Civ Eng 2005;17:143–52.
[12] Bludau C, Keuser M, Kustermann A. Perforation resistance of high-strength concrete panels. ACI Struct J 2006;103.
[13] Wille K, Naaman AE, El-Tawll S. Optimizing ultra-high-performance fiber-reinforced concrete. Concr Int 2011;33:35–41.
[14] Keppert M, Reiterman P, Pavlik Z, Pavlikova M, Jerman M, Cerny R. Municipal solid waste incineration ashes and their potential for partial replacement of Portland cement and fine aggregates in concrete. Cem Wapno Beton 2010;15:187.
[15] Hanchak S, Forrestal M, Young E, Ehrgott J. Perforation of concrete slabs with 48 MPa (7 ksi) and 140 MPa (20 ksi) unconfined compressive strengths. Int J Impact Eng 1992;12:1–7.
[16] Wuest J, Denarié E, Brühwiler E. Model for predicting the UHPFRC tensile hardening response. Kassel, Germany: Ultra High Performance Concrete; 2008. p. 153–60.
[17] Vossoughi F, Ostertag CP, Monteiro PJM, Johnson GC. Resistance of concrete protected by fabric to projectile impact. Cem Concr Res 2007;37:96–106.